# Efficient generation and extreme compression of multidimensional solitary states in molecular gas-filled hollow-core fibers driven by picosecond Yb lasers

Cite as: APL Photon. 10, 046112 (2025); doi: 10.1063/5.0252893 Submitted: 12 December 2024 • Accepted: 2 April 2025 •







**Published Online: 16 April 2025** 

Maghsoud Arshadipirlar,<sup>1</sup> Dipendra Khatri,<sup>2</sup> Stephen Londo,<sup>1</sup> Behnam Azizi,<sup>1</sup> Gaetan Jargot,<sup>1</sup> Mayank Kumar,<sup>1</sup> Chunmei Zhang,<sup>3</sup> Chelsea Kincaid,<sup>2,4</sup> Christopher Lantigua,<sup>2</sup> Tran-Chau Truong,<sup>2</sup> Heide Ibrahim,<sup>1,5</sup> Paul B. Corkum,<sup>3</sup> Michael Chini,<sup>2,6</sup> François Légaré,<sup>1</sup> and Reza Safaei,<sup>1,3,7,a)</sup>

#### **AFFILIATIONS**

- <sup>1</sup> Advanced Laser Light Source (ALLS), Institut National de la Recherche Scientifique (INRS-EMT), 1650 Boulevard Lionel-Boulet, Varennes, Québec, J3X 1P7, Canada
- Department of Physics, University of Central Florida, Orlando, Florida 32816, USA
- <sup>3</sup> Joint Attosecond Science Laboratory, University of Ottawa and National Research Council of Canada, 25 Templeton St., Ottawa, Ontario K1N 6N5, Canada
- <sup>4</sup>Linac Coherent Light Source, SLAC National Accelerator Laboratory, 2575 Sand Hill Road, MS103, Menlo Park, California 94025, USA
- <sup>5</sup> Department of Physics, University of Ottawa, 25 Templeton St., Ottawa, Ontario K1N 6N5, Canada
- Department of Physics, The Ohio State University, 191 W Woodruff Ave., Columbus, Ohio 43210, USA
- MPB Communications Inc. 147 Hymus Boulevard, Pointe-Claire, Québec, H9R 1E9, Canada

**Note:** This paper is part of the Special Topic on Advances enabled by Ytterbium: from Advanced Laser Technology to Breakthrough Applications.

a) Author to whom correspondence should be addressed: reza.safaei@inrs.ca

## **ABSTRACT**

We present an in-depth study on the impact of spatiotemporal Raman enhancement in molecular gas-filled hollow-core fibers (HCFs), demonstrating the efficient generation and post-compression of multidimensional solitary states (MDSS). Through different experimental scenarios—employing large-core HCFs filled with molecular gases (N<sub>2</sub> and N<sub>2</sub>O) and driven by high energy, sub-picosecond and picosecond Fourier transform-limited ytterbium laser pulses—this work leverages multimode propagation and enhanced spatiotemporal interactions to achieve significant spectral broadening and asymmetric redshift, contrasting sharply with self-phase modulation. Our findings reveal that, beyond the regime of maximum nonadiabatic molecular alignment, spatiotemporal nonlinear enhancement primarily governs spectral broadening for input pulse durations up to 1 ps. The process shows limited sensitivity to input pulse duration and the two investigated molecular gases (N<sub>2</sub> and N<sub>2</sub>O), with only subtle differences in broadening arising from their distinct Raman spectroscopic properties. Furthermore, post-compression of MDSS was achieved in various cases. Notably, using 7 mJ, 1 ps laser pulses, we generated 22 fs pulses with a 47% energy conversion efficiency of the input pulse energy. These results position MDSS as a powerful platform for generating high-energy, ultrashort pulses with tunable wavelengths, offering a robust solution for applications such as high harmonic generation.

© 2025 Author(s). All article content, except where otherwise noted, is licensed under a Creative Commons Attribution (CC BY) license (https://creativecommons.org/licenses/by/4.0/). https://doi.org/10.1063/5.0252893

#### I. INTRODUCTION

In recent years, there has been growing interest in diodepumped Yb-based laser systems. These lasers utilize innovative geometries, such as fibers, InnoSlabs, thin disks, and cryogenically cooled amplifiers, and have enabled the generation of ultrashort pulses with energies up to several hundreds of mJ, positioning them as promising candidates for next-generation high-power applications. Although Yb-based systems typically produce longer pulse durations due to their narrow emission bandwidth, their simpler cooling requirements and cost-effectiveness make them ideal for applications needing high-energy, high-repetition-rate lasers. These advantages make Yb lasers highly attractive for advanced laser-driven applications and offer great potential for laser-based plasma x-ray sources, inverse Compton scattering, acceleration of ultrarelativistic electron beams, high harmonics, and THz generation.

Most Yb-based lasers, such as Yb-doped fiber chirped pulse amplifiers, <sup>15-20</sup> Yb:KGW, <sup>21-24</sup> and Yb:CaF<sub>2</sub>, <sup>25,26</sup> typically operate with pulse durations of hundreds of femtoseconds, with pulse energies ranging from hundreds of microjoules to hundreds of millijoules (Fig. 1). Among them, CPA-based thin-disk Yb:YAG lasers are considered the state-of-the-art in modern laser technology, offering an outstanding combination of a high average power, high pulse energy, and excellent beam quality from the kHz to MHz repetition rate, typically with pulse durations in the ps range. <sup>27-31</sup> Subsequent

spectral broadening is, therefore, necessary to overcome their gain bandwidth limitations and meet the sub-50 fs requirements for applications such as ultrafast molecular spectroscopy and HHG. An ideal driver for high-power ultrafast applications must generate short pulses (tens of femtoseconds) with high energy (several mJ) and tunable wavelengths. <sup>12</sup> Although optical parametric amplification (OPA) and optical parametric chirped pulse amplification (OPCPA) are frequently used to produce such pulses, these methods are complex, often featuring multiple nonlinear amplification stages, and face limitations such as low conversion efficiency and imperfect beam quality. <sup>32,33</sup>

This has driven the demand for efficient compression techniques tailored to ultrashort pulses. One approach is nonlinear pulse compression, commonly referred to as the post-compression method. Techniques such as filamentation<sup>34</sup> and bulk material compression<sup>35</sup> have achieved notable results, including the compression of Yb-based laser pulses to 30 fs at the mJ level.<sup>36</sup> However, challenges such as plasma effects and optical damage limit scaling to higher energies. Recent advances in gas-filled multi-pass cells have enabled efficient pulse compression beyond the mJ range, <sup>37–39</sup> including the compression of ps Yb disk amplifiers<sup>29</sup> and the generation of few-cycle pulses.<sup>38</sup> For instance, a 1.3 ps Yb laser has been compressed to 37 fs at 100 mJ, <sup>31</sup> while sub-10 fs pulses have been achieved using two-stage multi-pass cells. <sup>40</sup> However, this technique requires precise dispersion control with chirped mirrors and can

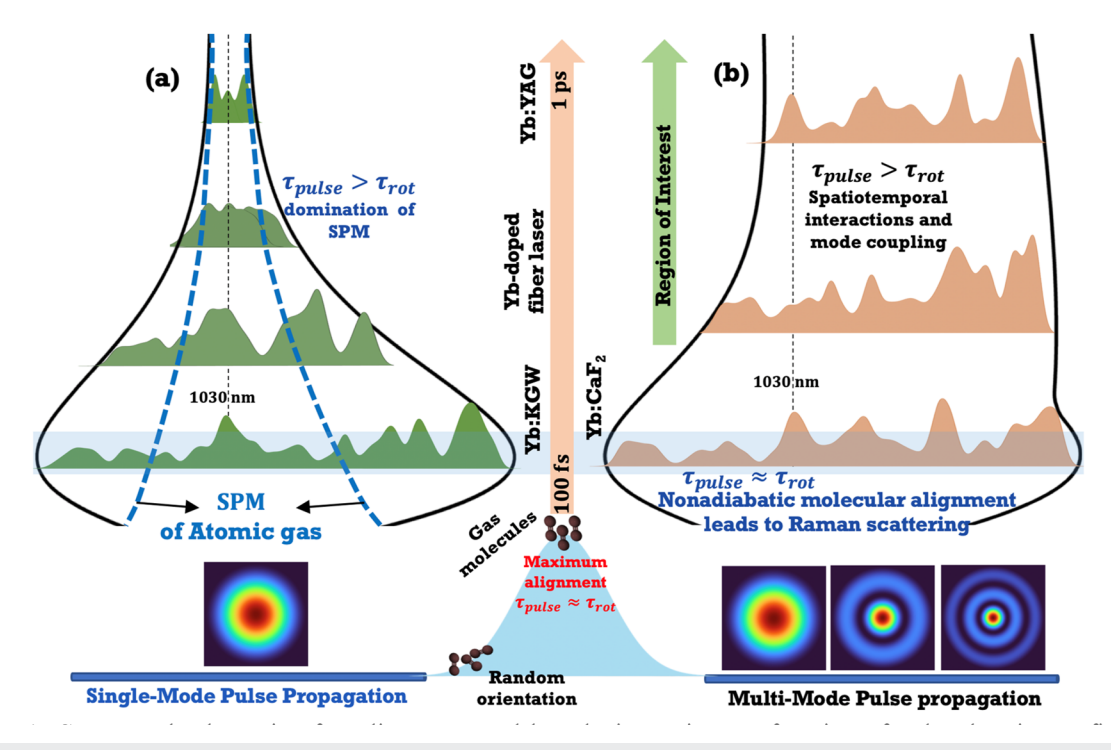


**FIG. 1.** Conceptual schematic of the nonlinear spectral broadening ratio as a function of pulse duration at fixed pressure and constant peak power for the specific fiber length. In single-mode propagation (a), molecular alignment theory predicts reduced spectral broadening ratio for pulse durations longer than the characteristic molecular rotational timescale,  $\tau_{rot}$  (which is highlighted by the shaded light blue horizontal bar). For longer pulses, the nonlinear propagation is dominated by SPM with a limited compression ratio (dashed blue curve). For multimode propagation (b), experimental observations in multimode propagation show a stark contrast, with efficient spectral broadening persisting beyond  $\tau_{rot}$  due to enhanced spatiotemporal interactions and mode coupling. The black curves represent the range of spectral broadening as a function of pulse duration for both single-mode and multimode propagation cases.

suffer from beam quality limitations at high energies, reducing the overall efficiency and stability of the compressed pulses. <sup>5,31</sup>

Over the past three decades, gas-filled HCF-based nonlinear compression techniques have consistently demonstrated the ability to generate high-energy, few-cycle pulses, initially with Ti:sapphire (Ti:Sa) lasers. 41,42 These methods typically involve nonlinear spectral broadening in gas-filled fibers, followed by spectral phase compensation through chirped mirrors or bulk materials.<sup>43</sup> torically, HCF-based compressors have utilized SPM to broaden ultrashort pulse spectra in noble gases. Using this method, sub-10 fs durations with mJ-level pulse energies have been reported for Ti:Sa lasers. 45,46 More recently, nonlinear pulse propagation in gas-filled HCFs has shown particular promise for producing high-energy, high-repetition-rate ultrashort pulses, especially when combined with Yb-based laser systems. 17,26 Significant pulse compression results, generating few-cycle pulses with sub-10 fs durations, have been achieved through moderately driving SPM over single-stage<sup>20-22</sup> and two-stage<sup>23,47</sup> noble gas-filled HCFs, for Ybbased lasers with initial pulse durations ranging from 150 to 300 fs. Despite its advantages in compressing ultrafast pulses, the method has limitations, with the compression ratio inherently restricted and requiring longer fibers or multiple stages for maximum compression. In addition, the spectral broadening ratio decreases with longer initial pulse durations (as shown in Fig. 1), making this approach less effective for lasers in the ps range.

Recent advancements have demonstrated the potential of molecular gases as highly efficient nonlinear media for spectral broadening. 48-52 Unlike noble gases, molecular gases exhibit a delayed nonlinear response due to molecular alignment and bond stretching under strong laser fields.<sup>53</sup> By tuning the input pulse duration to match the molecular rotational timescale, one can achieve efficient spectral broadening. In particular, N2O-filled HCFs have shown a record 45-fold compression, producing broad supercontinuum spectra ideal for few-cycle pulse generation.<sup>51</sup> However, 1D simulations suggest that for pulse durations beyond this timescale, spectral broadening diminishes greatly and becomes symmetric because SPM begins to dominate over Raman effects<sup>51</sup> [Fig. 1(a)]. This contrast is further highlighted by a clear discrepancy between the experimental results of input pulse duration scans and 1D simulation predictions.<sup>54</sup> A significant breakthrough occurred with the observation of multidimensional solitary states (MDSS) in nitrogen-filled HCFs, driven by sub-ps near-infrared pulses.<sup>49</sup> This regime, characterized by strong intermodal interactions and enhanced Raman nonlinearities, enables efficient broadband, redshifted multimode solitary states. Unlike 1D propagation, where spectral broadening reduces with longer pulse durations, MDSS in multimode fibers maintain efficient broadening through the combined effects of stimulated Raman scattering (SRS) and mode coupling.

As shown in Fig. 1(b), the multimode nature of gas-filled HCFs and spatiotemporal nonlinear enhancement due to the creation of stable multimode solitary states ensure efficient spectral broadening even as pulse duration increases.<sup>52</sup> This unique behavior makes molecular gas-filled HCFs as highly promising for nonlinear spectral broadening across a broad range of pulse durations, from 100 fs to ps, covering the typical operating range of the state-of-the-art Yb lasers. Despite earlier demonstrations using chirped pulses, no experimental evidence of MDSS

driven directly by transform-limited sub-ps or ps lasers has been reported.

In this paper, we demonstrate, for the first time, the efficient generation of MDSS using sub-ps and ps Yb-based laser systems, followed by extreme nonlinear compression. Using 700 fs and 1 ps pulses in molecular gas-filled HCFs, we generated MDSS, which were subsequently compressed to  $\sim\!20$  fs using simple dispersion compensation with bulk materials. Contrary to expectations based on 1D propagation, our experimental results indicate that for pulse durations up to 1 ps—covering the primary operating range of ultrafast Yb lasers—spatiotemporal nonlinear enhancement dominates spectral broadening, making it less sensitive to the input pulse duration in this regime. In addition, measurements with  $N_2$  and  $N_2O$  reveal that this enhanced nonlinearity is not strongly dependent on the gas type or its molecular timescale. This challenges the assumption that molecules with slower rotational response times necessarily lead to greater broadening for longer pulse durations.

#### II. RESULTS AND DISCUSSION

To realize experiments across a broad range of parameter space, experiments were conducted using multiple laser sources in different facilities, using both N2- and N2O-filled fibers with varying inner diameters. One of the experiments was conducted at the Advanced Laser Light Source (ALLS) user facility. The laser source was a Yb-based system (Amplitude, Magma), emitting 700 fs pulses at a central wavelength of 1030 nm and operating at a repetition rate of 1 kHz. The fiber was operated with a uniform static pressure, which was achieved by first evacuating the fiber using a vacuum pump and then by injecting the molecular gas (either N2 or N2O) into the fiber and allowing the system to equilibrate. The laser beam was focused into a stretched HCF (few-cycle Inc.) with a core diameter of 500  $\mu$ m and a length of 2.6 m. We measured the spectral broadening and energy of the output beam using a UV-Vis and NIR spectrometer, along with a power meter. The pulse duration, as well as the spectral and temporal phases of the output beam, was characterized using a home-built Second Harmonic Generation Frequency Resolved Optical Gating (SHG-FROG) setup (see the supplementary material for setup schematic). To further investigate the capabilities of the MDSS method, various spectral filters were applied to select specific bandwidths of the output spectra generated by the MDSS process. This allowed us to evaluate the temporal, spectral, and spatial characteristics of the output pulses.

We first investigated the effect of increasing pressure on the spectral broadening of input pulses in an  $N_2$  and  $N_2O$  gas-filled HCF. By maintaining a constant peak power at the fiber input ( $\sim$ 5.4 GW for the  $N_2$  experiment and  $\sim$ 0.67 GW for the  $N_2O$  experiment), we recorded the spectral broadening across different gas pressures in the static regime for both  $N_2$  and  $N_2O$  gases. The dependence of spectral broadening on the injected  $N_2$  and  $N_2O$  gas pressure is illustrated in Figs. 2(a) and 2(b). In both cases, we observed a significant redshift in spectral broadening. According to Safaei *et al.*,<sup>49</sup> the MDSS generation involves coupling the beam into high-order modes (HOMs) near the fiber input via self-focusing, leading to intermodal four-wave mixing (IFWM) and the generation of new frequencies. Once the bandwidth of these new frequencies overlaps with the Raman gain, intermodal SRS occurs. This process produces highly spatiotemporally localized solitary pulses

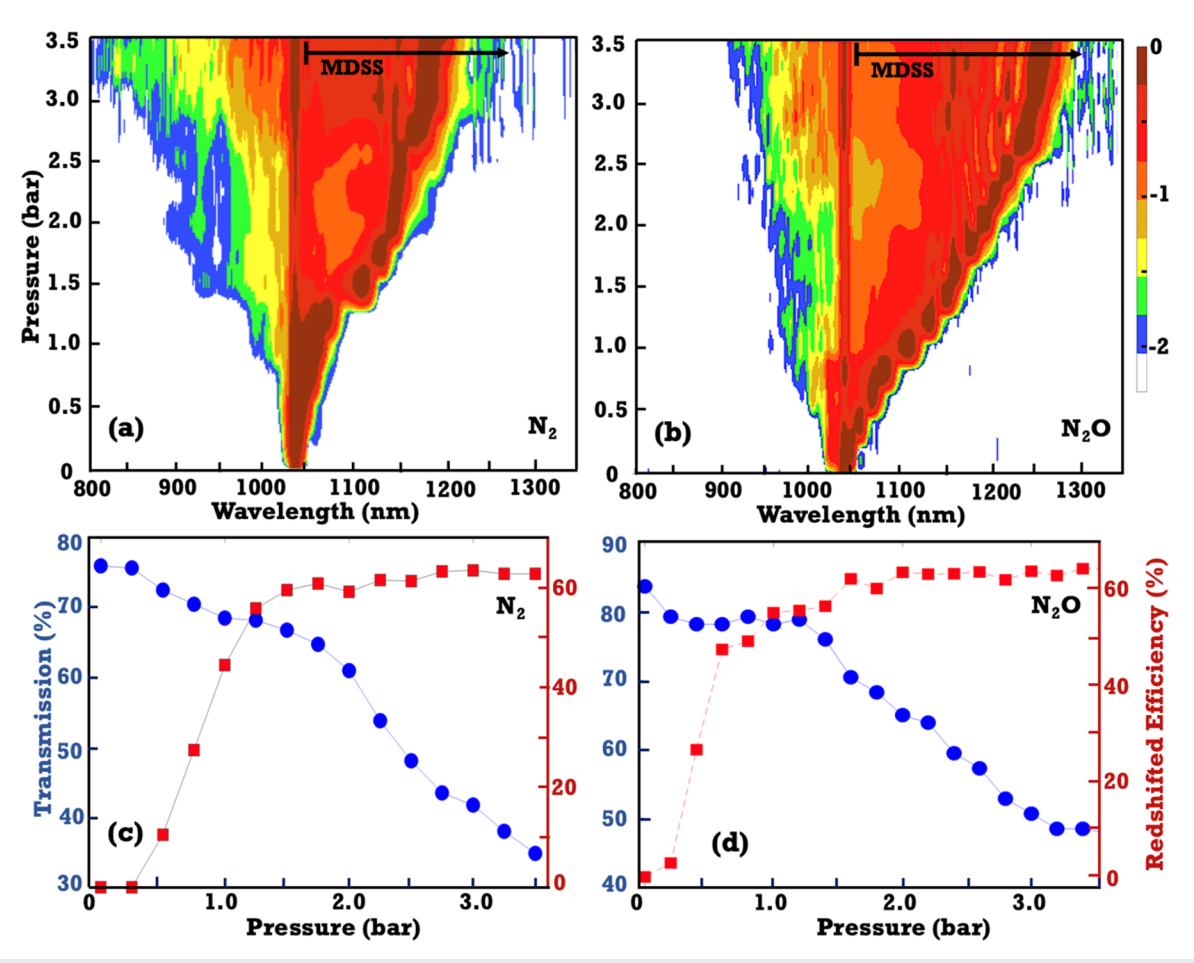


FIG. 2. Spectral broadening as a function of pressure for  $N_2$  (a) and  $N_2O$  (b) gases. Input pulse energies were 4 mJ for  $N_2$  and 0.5 mJ for  $N_2O$ . Panels (c) and (d) show the fiber transmission (blue circles) and the energy transmitted to the redshifted region (MDSS energy) (red squares) for  $N_2$  and  $N_2O$ , respectively.

as a result of intermodal interactions that balance diffraction and dispersion.  $^{49-52}$  Therefore, in the MDSS, strong intermodal interactions induce enhanced Raman nonlinearity in the large-core HCF, resulting in broadband redshifted spectra, which is evident in the spectral scans of both  $N_2O$  and  $N_2$  gases. In addition, as pressure increases, the enhanced nonlinearity of the medium amplifies the Raman gain, leading to more spectral broadening.

Figures 2(c) and 2(d) illustrate the fiber transmission and the percentage of the output beam energy in the redshifted region (calculated as redshifted energy/output energy×100) using a 1050 nm spectral filter for  $N_2$  and  $N_2O$  gases, respectively. The data clearly show that increasing the gas pressure reduces fiber transmission for both gases. This decline can be attributed to the fact that, as the pressure increases, the input pulse peak power approaches the critical power for self-focusing. In a static configuration, phenomena such as Kerr lensing likely occur before coupling to the fiber, reducing coupling efficiency and, consequently, fiber transmission. Despite this, the experimental results indicate that the energy transferred to the redshifted region, which corresponds to the MDSS, increases with

rising gas pressure, reaching a peak of  $\sim$ 62% for  $N_2$  and 65% for  $N_2$ O. Beyond this point, further pressure increases cause the energy transfer to the redshifted region to plateau even though the fiber transmission continually decreases. This finding is remarkable, as it demonstrates that while the total fiber transmission decreases with increased pressure, the efficiency of energy transfer from the main beam to the MDSS part does not decline. This behavior suggests that a portion of the input energy is transferred to the MDSS region early in the fiber, where it undergoes soliton frequency shifts and spectral broadening. The energy loss from the main beam does not affect the MDSS in the remaining length of the fiber. As a result, even as the overall fiber transmission decreases, the spectral broadening persists, driven by increasing the gas pressure and nonlinearity and the sustained energy transfer to the redshifted part of the spectrum.

As mentioned, in molecular gases, the SRS mechanism introduces nonlinear effects due to the rotational degrees of freedom. These effects are the result of the laser field exerting a torque on the molecular frame, aligning it with the direction of the field. Longer laser pulses increase the degree of molecular alignment,

thus enhancing nonlinearity. At the same time, the molecular alignment response is delayed compared with the pulse, which causes the spectrum to shift predominantly toward the longer wavelength. Theoretically and experimentally, it has been shown that the optimal pulse durations for achieving the broadest spectral bandwidth are around 150 fs for N<sub>2</sub> and 280 fs for N<sub>2</sub>O. 50-52 In this study, we used 700 fs pulses, which are longer than the optimal duration for maximizing spectral broadening in N2 and N2O. It is particularly interesting to observe how the spectral broadening behaves when we are far from the optimal pulse duration for nonadiabatic alignment. A key question arises: Will N2O experience more broadening due to its slower response time when the pulse accumulates the same nonlinear B integral for both gases? This question is critical because the molecular alignment and rotational dynamics of  $N_2\mathrm{O}$ occur over a longer timescale compared with those of N2. Under the same nonlinear conditions, the slower response of N2O could lead to more pronounced spectral broadening, as the delayed nonlinearities, such as Raman scattering, may have a stronger impact over the pulse duration. Exploring this behavior can provide insights into the role of molecular response times in shaping the nonlinear dynamics of spectral broadening, especially when operating away from the optimal pulse duration for nonadiabatic alignment.

The nonlinearity of the materials at different wavelengths is defined by the B-integral:

$$B = k_0 \int_0^L n_2 I(z) dz \approx \frac{2\pi n_2 I_{\text{max}} L}{\lambda_0}, \tag{1}$$

where  $n_2$  is the nonlinear refractive index,  $I_{\rm max}$  is the on-axis peak intensity of the laser pulse, and L is the effective length of the material. To maintain a constant B-integral, we kept  $\lambda_0$  and L the same for both gases. Thus, to have the same B-integral, the condition  $(n_2I)_{N_2} = (n_2I)_{N_2O}$  must be satisfied. Nonlinear refractive index values for  $N_2$  and  $N_2O$  are primarily derived from Ref. 55 for pulse durations near the rotational alignment time frames. For longer pulse durations, such as the 700 fs pulses used in this study, we apply the following equation to estimate the effective nonlinear refractive index  $(n_{2,eff})$ :<sup>56</sup>

$$n_{2,eff} = n_{2,el} + n_{2,rot} (1 - \exp(-\tau/\tau_0)),$$
 (2)

where  $n_{2,el}$  and  $n_{2,rot}$  correspond to pure electronic and rotational nonlinearities and  $\tau_0$  is a characteristic response time. Based on this approach, the ratio of  $n_{2,eff}$  for  $N_2O$  and  $N_2$  at 700 fs is calculated to be ~13. Therefore, by selecting  $I_{N_2}=13$   $I_{N_2O}$  at a specific pressure, we can approximate the B-integral as being the same for both gases. Under these conditions, we were able to compare the spectral broadening and the efficiency of energy transmission to the redshifted regions in both gases.

As shown in Fig. 3(a), while the overall spectral broadening is comparable for both N2 and N2O, subtle differences in the spectral shapes can be observed. These differences arise from the distinct molecular properties and nonlinear responses of the two gases, particularly the slower rotational response time and higher Raman gain coefficient of N2O, which influence the spectral broadening dynamics slightly and lead to a modest difference in the redshifted spectra under the experimental conditions. Figure 3(b) demonstrates that the energy transmission efficiency remains comparable across various pressures. However, at higher pressures, the energy transmission efficiency to the red part of the spectrum is slightly more pronounced in N2O compared with N2. This effect can be attributed to the higher Raman gain coefficient in N2O in comparison with N2 gas for this pulse duration. These results reveal that the spectral broadening is less affected by the type of gas, despite differences in the molecular properties and Raman gain coefficients of N2 and N2O. In addition, they suggest that in the regime away from maximum nonadiabatic molecular alignment, spectral broadening remains relatively insensitive to the input pulse duration up to 1 ps, in contrast to broadening dominated by SPM. This highlights the significant role of spatiotemporal Raman enhancement in shaping the observed dynamics, even for longer laser pulses in this unique regime of gas-filled HCFs.

To further elucidate the nature of the mentioned spatiotemporal nonlinear behavior, we examine the spectral broadening and beam profiles of different spectral regions for both  $N_2$  [Fig. 4(a)] and  $N_2O$  [Fig. 4(b)] gases at a pressure of 3 bar. In the case of  $N_2$  gas, the input pulse energy was 5 mJ, and for  $N_2O$  gas, the input pulse energy was 0.4 mJ, with the same HCF (2.6 m length and 500  $\mu$ m

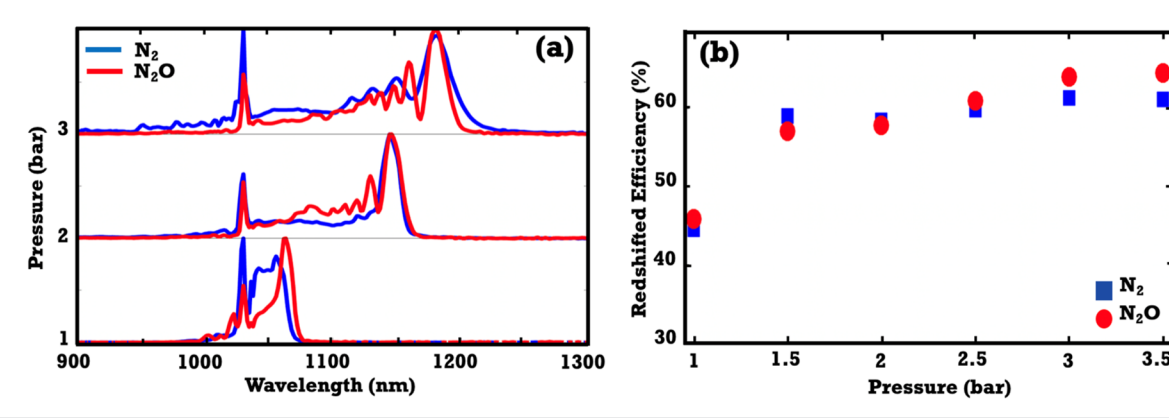
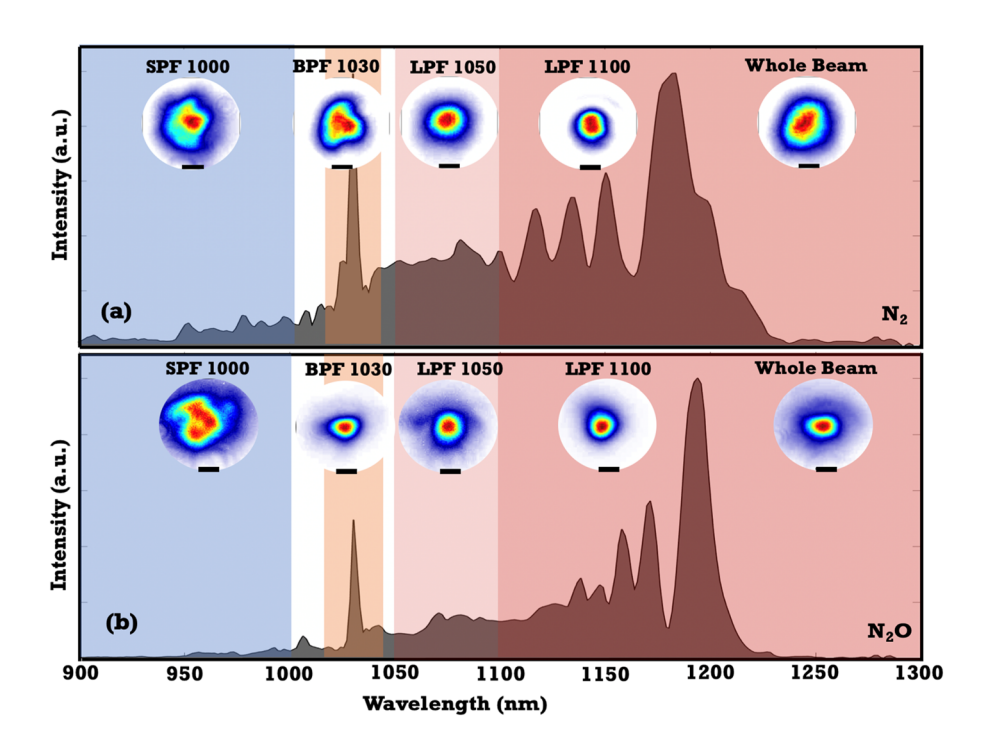


FIG. 3. Comparison of spectral broadening (a) and the efficiency of energy transfer to the redshifted part (b) for  $N_2$  and  $N_2O$  gases at different pressures, maintaining a constant B-integral for both gases. The input pulse energy is 4 mJ for  $N_2$  and 0.3 mJ for  $N_2O$ .



**FIG. 4.** Spectral broadening and beam profiles for  $N_2$  (a) and  $N_2O$  (b) gases at a pressure of 3 bar. In (a), 5 mJ input pulses are used with  $N_2$  gas, while in (b), 0.4 mJ laser pulses are applied with  $N_2O$  gas. The scale bar represents 200  $\mu$ m.

core diameter) used in both experiments. To capture spatial profiles, we used a short-pass filter (SPF) with a cutoff wavelength of 1000 nm for the blueshifted spectra, a bandpass filter (BPF) centered at 1030 ± 10 nm for the fundamental beam, and long-pass filters (LPFs) with cut-on wavelengths of 1050 and 1100 nm for the various redshifted spectral regions. For both cases, in the blueshifted region that occurs in the trailing edge of the pulses, there is a lack of self-organization, leading to rapid power exchange between higher-order modes and subsequent beam instability. Figure S2 of the supplementary material presents 15 consecutive beam profiles of the blueshifted region for  $N_2O$  gas. These results show that the beam profile for the blueshifted spectral range (900-1000 nm) exhibits regions of both self-focusing and strong divergence, further emphasizing the intrinsic instability in this region. This instability arises due to the lack of the Raman gain, which leads to a nonuniform and unstable beam profile. Although ionization or harmonic generation may introduce additional perturbations, their contribution is minor compared with the dominant spatiotemporal instability in this region. However, in the redshifted region associated with the MDSS, the beam profile is observed to be spatially clean and stable. Here, we observe that the spectral broadening due to MDSS results in a redshifted output beam with a high spatial profile quality.

To characterize the broadband, redshifted MDSS output, we employed SHG-FROG. Figures 5(a)-5(h) present experimental and reconstructed spectrograms, as well as their corresponding spectra from the FROG results and the temporal profile of the pulses after the post-compression for N<sub>2</sub> and N<sub>2</sub>O gases under the conditions described in Fig. 4. For this pulse characterization, we used a LPF with a cutoff wavelength of 1050 nm to isolate the MDSS portion of the spectra. Our results indicate that for the N<sub>2</sub> case, considering the dispersion of the gas within the output tube of the setup, a 5 mm

vacuum system output window, a 0.5 mm collimating lens, and 5 m of air propagation, the output pulse duration reached ~62 fs, indicating partial compression. Given the characteristic negative frequency chirp of the MDSS output, <sup>49,50</sup> we utilized an extra 12 mm-thick BaF<sub>2</sub> window providing positive group velocity dispersion (GVD) in the relevant wavelength range to further compress the output pulses. This choice was made to effectively compensate for the negative chirp and achieve optimal pulse compression, resulting in a pulse duration of 24 fs, with a pulse energy of 1.3 mJ and a central wavelength of 1150 nm. The peak power of this pulse reached ~46 GW (by considering a Gaussian beam shape and 10% of pedestal). Achieving this pulse involved focusing a 4 mJ Yb-based laser pulse into the HCF filled with N2 gas at 2 bar pressure. In this configuration, the fiber transmission was ~52%, yielding 2.1 mJ at the output. Approximately 62% of this output pulse energy is transferred to the MDSS part, with a central wavelength of 1150 nm and a pulse duration of 24 fs. In the case of N2O gas, we characterized the output pulse at 2 bar pressure using an input laser pulse with an energy of 0.5 mJ. For this pulse characterization, we selected the MDSS portion of the spectrum using an LPF with a cut-on wavelength of 1100 nm. In this case, we achieved a pulse duration of 19 fs with a central wavelength of 1200 nm. To compress this pulse, we used 9 mm-thick BaF<sub>2</sub> windows. The energy of the output pulses in the MDSS part, measured with a spectral filter with a cutoff wavelength of 1100 nm, was 100 µJ. In gas-filled HCFs, modal dispersion and losses scale inversely with the second and third power of the core size, respectively. Consequently, large-core HCFs provide ultralow modal dispersion and minimal losses. In the high-energy regime, due to self-focusing and diffraction effects, multiple modes can be created at the fiber's input. These multidimensional pathways enhance the nonlinear effects, including SRS, throughout the propagation in the

19 June 2025 18:12:4:

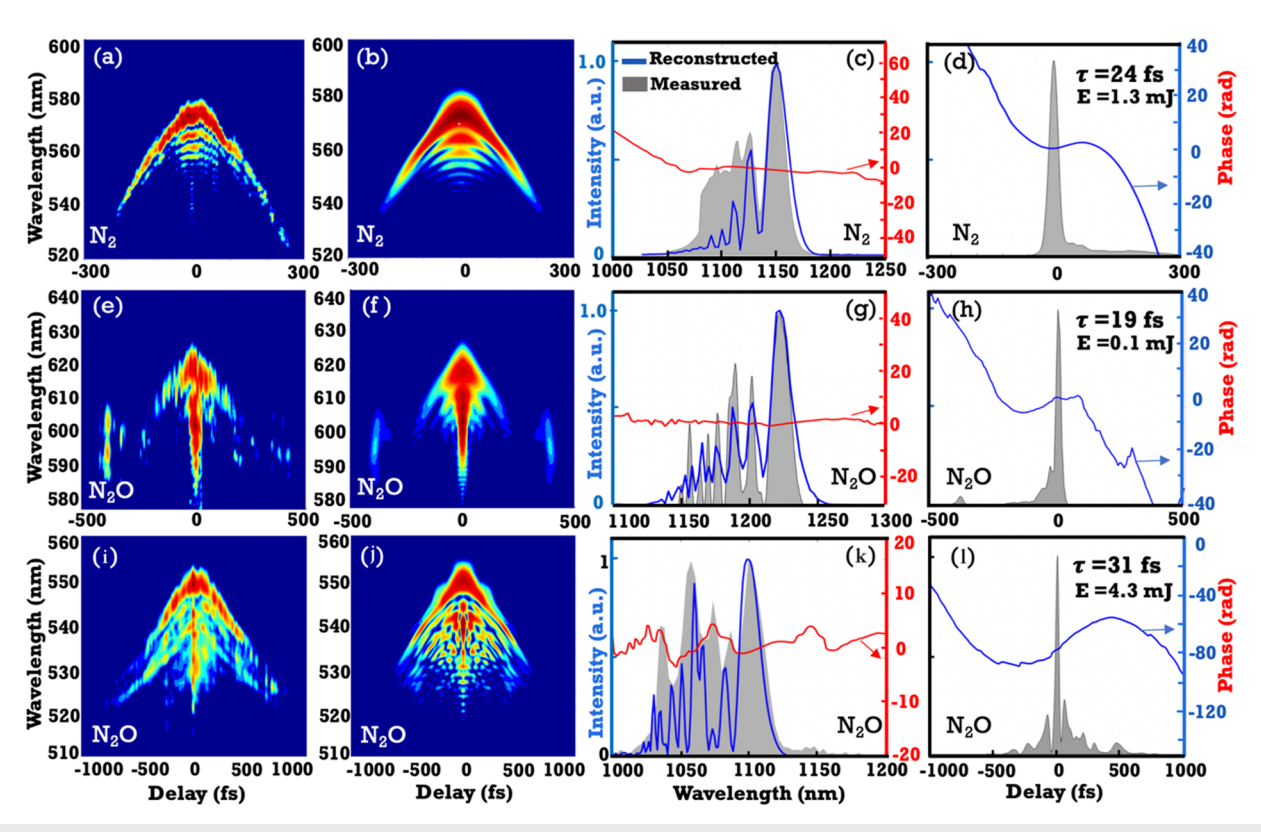


**FIG. 5.** Experimental [(a), (e), and (i)] and reconstructed [(b), (f), and (j)] spectrograms, along with the corresponding experimental (filled gray) and reconstructed (blue line) spectra [(c), (g), and (k)] and the retrieved temporal intensity profiles of the compressed pulses [(d), (h), and (l)] for  $N_2$  and  $N_2$ O gases.  $\tau$  is the duration, and E is the energy of the reconstructed pulse.

HCF. Therefore, we employed a larger-core fiber (750  $\mu$ m) with reduced modal dispersion and filled it with N2O gas at a very low pressure of 250 mbar to explore energy scaling. With a high input energy of 6 mJ per pulse, we achieved notable spectral broadening at the fiber output (see the supplementary material, Fig. S3), which was subsequently compressed to a pulse duration of 30 fs. Figures 5(i) and 5(j) illustrate the experimental and reconstructed spectrograms of the output pulses, while Fig. 5(k) shows the experimental and retrieved spectra. The corresponding temporal profile of the compressed pulses is displayed in Fig. 5(1). Thus, this method is a pathway for energy scaling in HCF systems. The results demonstrate that by using the larger core HCF or selecting a molecular gas with a high ionization threshold, such as N2, it is possible to increase the input pulse energy to generate high-energy, short-duration pulses with a tunable central wavelength at the output of a large HCF, even when using longer input pulse durations (more than 700 fs).

Finally, we explored an alternative approach to demonstrate that pulses generated through spatiotemporal nonlinearity are largely independent of the input pulse duration. Even with longer pulse durations, we achieved comparable results. For this second set of experiments, we utilized a Yb laser based on thin-disk technology (Dira 200-1, Trumpf Scientific Laser), located at the Advanced Research Complex (ARC), with an output centered at 1030 nm and producing 1 ps pulses at 1 kHz repetition rate. We focused these

pulses with an energy of 7 mJ in a 2 m-long 500  $\mu m$  core diameter  $N_2$  gas-filled HCF. Note that in this case, we employed a differential pressure scheme, where the fiber is evacuated at the entrance while molecular gas is injected from the output end. This setup creates a pressure gradient along the fiber length to mitigate Kerr lensing at the fiber input and prevents a reduction in fiber transmission as pressure increases. The total fiber transmission was ~80%, and we did not observe a significant drop in transmission, even as the pressure was increased to 4 bar.

Figure 6 presents the results used to characterize the output pulses. Figures 6(a) and 6(b) show the experimental and reconstructed spectrograms, while Fig. 6(c) compares the input and output pulse spectra along with the reconstructed spectra. An LPF with a cut-on wavelength of 1050 nm was used for pulse characterization via SHG-FROG. The Wigner function of the retrieved experimental SHG-FROG trace [Fig. 6(e)] indicates a significant negative quadratic spectral phase at the leading edge of the output pulse, which contains most of the energy. Therefore, we used a 14 mm calcium fluoride (CaF<sub>2</sub>) window to compress the output pulse, achieving a pulse duration of 22 fs [Fig. 6(d)] with a clean, stable beam profile [Fig. 6(g)]. This process resulted in 2.8 mJ of energy (~47% efficiency with respect to input pulse energy) in the redshifted region, with a central wavelength of 1200 nm. In this case, the output pulse was ~45 times shorter than the input pump pulse.

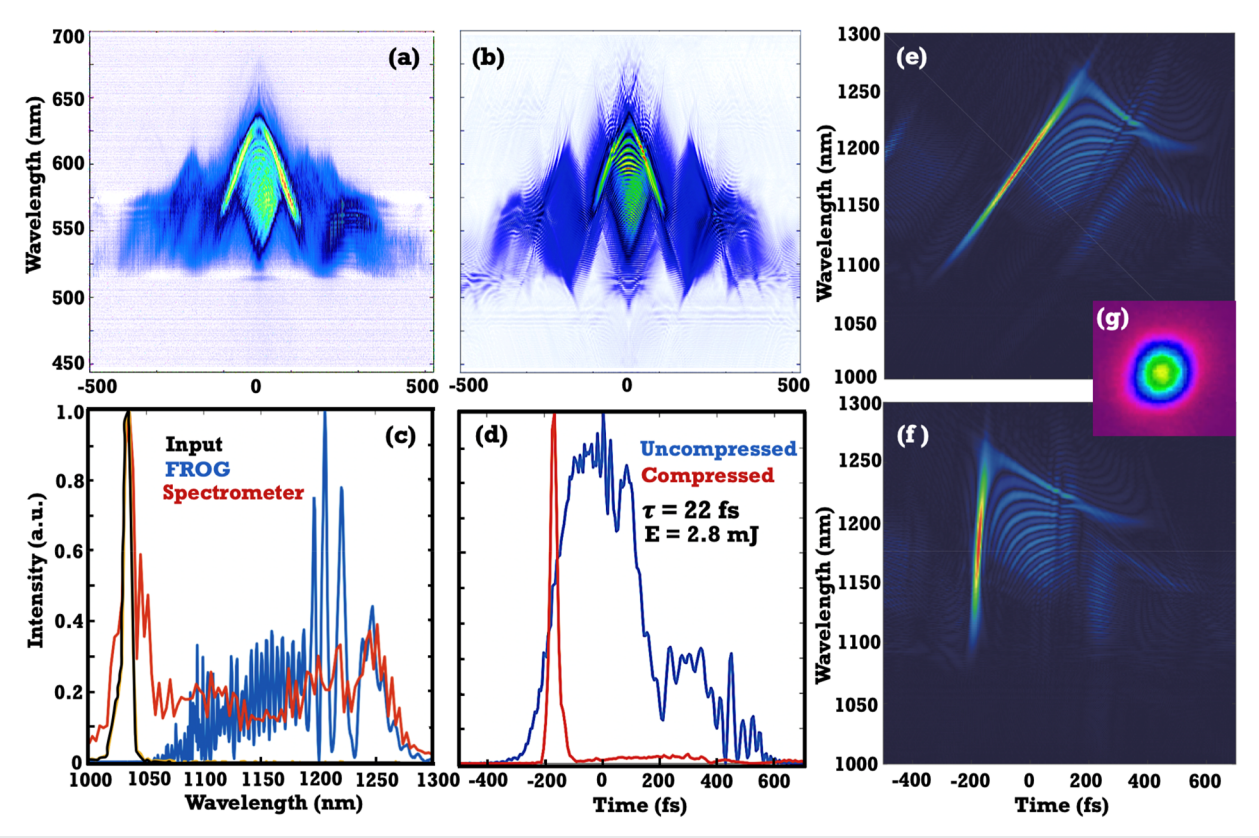


FIG. 6. Experimental (a) and reconstructed (b) spectrograms, experimental and reconstructed spectra (c), and temporal intensity profiles of the uncompressed and compressed pulses (d) for N<sub>2</sub> gas at 4 bar pressure and a high input pulse energy (7 mJ), with a 1 ps input pulse duration. The Wigner functions of the uncompressed (e) and compressed (f) output pulses are shown, along with the output beam profile (g).

The Wigner function of the compressed pulse [Fig. 6(f)] shows that the pulse is free of chirp, indicating successful compensation of the negative quadratic spectral phase with the CaF<sub>2</sub> window.

# III. CONCLUSION

In this study, we have demonstrated the generation and characterization of MDSS generated with picosecond and sub-picosecond Yb pulses within an HCF filled with molecular gases, specifically N<sub>2</sub> and N2O. By systematically varying gas pressure and input pulse energy, we observed a pronounced impact on spectral broadening and energy transmission. The experimental results underline the importance of optimizing experimental parameters to achieve desired outcomes in fine-tuning the central wavelengths of highenergy ultrafast laser systems. We demonstrated that the efficiency of spectral broadening in MDSS is less sensitive to both the input pulse duration (up to 1 ps) and the type of gas used [at least for the two investigated gases: N2 and N2O)] when driven by a pump with a pulse duration longer than the characteristic molecular alignment time. Our experimental results show that both N<sub>2</sub> and N<sub>2</sub>O behave similarly, with comparable spectral broadening and energy transfer efficiencies to the redshifted region when the system's nonlinearity is maintained by adjusting the B-integral for a pulse duration of around 700 fs. Here, unlike in single-mode propagation, the

enhanced spatiotemporal interactions and mode coupling of the system enhance nonlinear effects, allowing for more significant spectral shifts even with longer pulses. In addition, we showed that this enhancement becomes even more pronounced in larger core fibers, where, despite using very low gas pressures, we still observed significant spectral broadening and effective post-compression. Our results also indicated that even with a longer pulse duration (1 ps), we can achieve significant spectral broadening, and the output pulse can be further compressed to 22 fs (45-fold compression), with a central wavelength of 1200 nm and an energy conversion efficiency of 47%. This highlights the versatility of our approach, offering pathways for further exploration in laser technology and nonlinear optics. Our findings not only confirm the feasibility of generating stable MDSS for HCFs filled with molecular gases but also establish their potential for advanced applications, paving the way for future research in this exciting field. Moreover, our results provide a promising way to generate short pulses driven by ps Yb laser systems with doubles or triples of frequency. In an appropriate Raman-active gas-filled fiber, the MDSS process can be driven at 515 nm and perhaps even 343 nm. The method thus provides a straightforward and reliable nonlinear frequency conversion technique to generate tunable ultrashort pulses in the UV-Vis spectral region.

19 June 2025 18:12:4:

#### SUPPLEMENTARY MATERIAL

The supplementary material provides details on the experimental setup and experimental spectral broadening results as a function of input pulse energy for  $N_2O$  gas with low pressures.

#### **ACKNOWLEDGMENTS**

The authors acknowledge the Natural Sciences and Engineering Research Council of Canada (NSERC), the Canada Foundation for Innovation (CFI), PROMPT, the National Research Council of Canada's (NRC) "Quantum Sensors Program (QSP)," the U.S. Department of Energy (DOE), Office of Science, Basic Energy Sciences (BES), Award No. DE-SC0019291 (T.-C.T. and C.L.), the U.S. Department of Energy (DOE), Office of Science, Fusion Energy Sciences (FES), Award No. DE-SC0022540 (D.K.), and the Air Force Office of Scientific Research (AFOSR), Award No. FA9550-16-1-0149 (M.C. and C.K.).

## **AUTHOR DECLARATIONS**

#### **Conflict of Interest**

The authors have no conflicts to disclose.

#### **Author Contributions**

M.A. and D.K. contributed equally to this work.

Maghsoud Arshadipirlar: Conceptualization (equal); Data curation (equal); Formal analysis (equal); Methodology (equal); Software (equal); Visualization (equal); Writing - original draft (equal); Writing - review & editing (equal). Dipendra Khatri: Data curation (equal); Formal analysis (equal); Methodology (equal); Software (equal); Writing - original draft (equal); Writing - review & editing (equal). Stephen Londo: Data curation (equal); Writing – review & editing (equal). Behnam Azizi: Data curation (equal); Writing review & editing (equal). Gaetan Jargot: Writing - review & editing (equal). Mayank Kumar: Data curation (supporting); Writing - review & editing (equal). Chunmei Zhang: Data curation (equal). Chelsea Kincaid: Data curation (equal). Christopher Lantigua: Investigation (equal). Tran-Chau Truong: Software (supporting). Heide Ibrahim: Writing - review & editing (equal). Paul B. Corkum: Supervision (supporting). Michael Chini: Funding acquisition (equal); Methodology (equal); Supervision (equal); Writing review & editing (equal). François Légaré: Funding acquisition (equal); Supervision (equal); Writing - review & editing (equal). Reza Safaei: Formal analysis (equal); Investigation (equal); Methodology (equal); Project administration (equal); Validation (equal); Writing – original draft (equal); Writing – review & editing (equal).

# DATA AVAILABILITY

The data that support the findings of this study are available from the corresponding author upon reasonable request. The data are not publicly available.

## **REFERENCES**

<sup>1</sup>H. Stark, J. Buldt, M. Müller, A. Klenke, A. Tünnermann, and J. Limpert, "23 mJ high-power fiber CPA system using electro-optically controlled divided-pulse amplification," Opt. Lett. **44**, 5529–5532 (2019).

- <sup>2</sup>B. E. Schmidt, A. Hage, T. Mans, F. Légaré, and H. J. Wörner, "Highly stable, 54 mJ Yb-InnoSlab laser platform at 05kW average power," Opt. Express 25, 17549–17555 (2017).
- <sup>3</sup>T. Nubbemeyer, M. Kaumanns, M. Ueffing, M. Gorjan, A. Alismail, H. Fattahi, J. Brons, O. Pronin, H. G. Barros, Z. Major, T. Metzger *et al.*, "1 kW, 200 mJ picosecond thin-disk laser system," Opt. Lett. **42**, 1381–1384 (2017).
- <sup>4</sup>C. Baumgarten, M. Pedicone, H. Bravo, H. Wang, L. Yin, C. S. Menoni, J. J. Rocca, and B. A. Reagan, "1 J, 05 kHz repetition rate picosecond laser," Opt. Lett. **41**, 3339–3342 (2016).
- <sup>5</sup>H. Fattahi, H. G. Barros, M. Gorjan, T. Nubbemeyer, B. Alsaif, C. Y. Teisset, M. Schultze, S. Prinz, M. Haefner, M. Ueffing, A. Alismail, L. Vámos, A. Schwarz, O. Pronin, J. Brons, X. T. Geng, G. Arisholm, M. Ciappina, V. S. Yakovlev, D. E. Kim, A. M. Azzeer, N. Karpowicz, D. Sutter, Z. Major, T. Metzger, and F. Krausz, "Third-generation femtosecond technology," Optica 1, 45–63 (2014).
- <sup>6</sup>Y. Pfaff, G. Barbiero, M. Rampp, S. Klingebiel, J. Brons, C. Y. Teisset, H. Wang, R. Jung, J. Jaksic, A. H. Woldegeorgis, M. Trunk *et al.*, "Nonlinear pulse compression of a 200 mJ and 1 kW ultrafast thin-disk amplifier," Opt. Express 31, 22740–22756 (2023).
- <sup>7</sup>R. Keenan, J. Dunn, P. K. Patel, D. F. Price, R. F. Smith, and V. N. Shlyaptsev, "High-repetition-rate grazing-incidence pumped X-ray laser operating at 18.9 nm," Phys. Rev. Lett. **94**, 103901 (2005).
- <sup>8</sup>W. S. Graves, J. Bessuille, P. Brown, S. Carbajo, V. Dolgashev, K.-H. Hong, E. Ihloff, B. Khaykovich, H. Lin, K. Murari, E. A. Nanni, G. Resta, S. Tantawi, L. E. Zapata, F. X. Kärtner, and D. E. Moncton, "Compact x-ray source based on burst-mode inverse Compton scattering at 100 kHz," Phys. Rev. ST Accel. Beams 17, 120701 (2014).
- <sup>9</sup>M. G. Ronga, M. Cavallone, A. Patriarca, A. M. Leite, P. Loap, V. Favaudon, G. Créhange, and L. de Marzi, "Back to the future: Very high-energy electrons (VHEEs) and their potential application in radiation therapy," Cancers 13, 4942 (2021).
- <sup>10</sup>T. Kurz, T. Heinemann, M. F. Gilljohann, Y. Y. Chang, J. P. Couperus Cabadağ, A. Debus, O. Kononenko, R. Pausch, S. Schöbel, R. W. Assmann, M. Bussmann, H. Ding, J. Götzfried, A. Köhler, G. Raj, S. Schindler, K. Steiniger, O. Zarini, S. Corde, A. Döpp, B. Hidding, S. Karsch, U. Schramm, A. Martinez de la Ossa, and A. Irman, "Demonstration of a compact plasma accelerator powered by laser-accelerated electron beams," Nat. Commun. 12, 2895 (2021).
- <sup>11</sup>T. Popmintchev, M. C. Chen, D. Popmintchev, P. Arpin, S. Brown, S. Ališauskas, G. Andriukaitis, T. Balčiunas, O. D. Mücke, A. Pugzlys, A. Baltuška *et al.*, "Bright coherent ultrahigh harmonics in the keV x-ray regime from mid-infrared femtosecond lasers," Science **336**, 1287–1291 (2012).
- <sup>12</sup> K. Légaré, R. Safaei, G. Barrette, L. Arias, P. Lassonde, H. Ibrahim, B. Vodungbo, E. Jal, J. Lüning, N. Jaouen, Z. Tao, A. Baltuška, F. Légaré, and G. Fan, "Raman red-shift compressor: A simple approach for scaling the high harmonic generation cut-off," Adv. Photonics Res. 2, 2100113 (2021).
- <sup>13</sup>C. Millon, S. Houver, and C. J. Saraceno, "400 kHz repetition rate THz-TDS with 24 mW of average power driven by a compact industrial Yb-laser," Opt. Express 31, 7922–7932 (2023).
- <sup>14</sup>S. Mansourzadeh, T. Vogel, A. Omar, M. Shalaby, M. Cinchetti, and C. J. Saraceno, "Broadband, high power THz source at 540 kHz using organic crystal BNA," APL Photonics 8, 011301 (2023).
- <sup>15</sup>L. Arias *et al.*, "Few-cycle Yb laser source at 20 kHz using multidimensional solitary states in hollow-core fibers," Opt. Lett. 47, 3612–3615 (2022).
- <sup>16</sup> F. Guichard, A. Giree, Y. Zaouter, M. Hanna, G. Machinet, B. Debord, F. Gérôme, P. Dupriez, F. Druon, C. Hönninger, E. Mottay *et al.*, "Nonlinear compression of high energy fiber amplifier pulses in air-filled hypocycloid-core Kagome fiber," Opt. Express 23, 7416–7423 (2015).
- <sup>17</sup>L. Lavenu, M. Natile, F. Guichard, Y. Zaouter, M. Hanna, E. Mottay, and P. Georges, "High-energy few-cycle Yb-doped fiber amplifier source based on a single nonlinear compression stage," Opt. Express 25, 7530–7537 (2017).
- $^{18}$ E. Vicentini, Y. Wang, D. Gatti, A. Gambetta, P. Laporta, G. Galzerano, K. Curtis, K. McEwan, C. R. Howle, and N. Coluccelli, "Nonlinear pulse compression to 22 fs at 15.6  $\mu J$  by an all-solid-state multipass approach," Opt. Express 28, 4541–4549 (2020).
- <sup>19</sup>L. Lavenu, M. Natile, F. Guichard, Y. Zaouter, X. Delen, M. Hanna, E. Mottay, and P. Georges, "Nonlinear pulse compression based on a gas-filled multipass cell," Opt. Lett. 43, 2252–2255 (2018).

- <sup>20</sup>T. Nagy, S. Hädrich, P. Simon, A. Blumenstein, N. Walther, R. Klas, J. Buldt, H. Stark, S. Breitkopf, P. Jójárt, and I. Seres, "Generation of three-cycle multi-millijoule laser pulses at 318 W average power," Optica 6, 1423–1424 (2019).
- <sup>21</sup> Y. G. Jeong, R. Piccoli, D. Ferachou, V. Cardin, M. Chini, S. Hädrich, J. Limpert, R. Morandotti, F. Légaré, B. E. Schmidt, and L. Razzari, "Direct compression of 170-fs 50-cycle pulses down to 1.5 cycles with 70% transmission," Sci. Rep. 8, 11794 (2018).
- <sup>22</sup>Z. Pi, H. Y. Kim, and E. Goulielmakis, "Petahertz-scale spectral broadening and few-cycle compression of Yb:KGW laser pulses in a pressurized, gas-filled hollowcore fiber," Opt. Lett. 47, 5865–5868 (2022).
- <sup>23</sup> N. Ishii and R. Itakura, "Sub-two-cycle intense pulse generation based on two-stage hollow-core fiber compression using an ytterbium amplifier," Appl. Phys. Express 17, 042006 (2024).
- $^{24}$ j. E. Beetar, S. Gholam-Mirzaei, and M. Chini, "Spectral broadening and pulse compression of a 400  $\mu$ J, 20 W Yb:KGW laser using a multi-plate medium," Appl. Phys. Lett. **112**, 051102 (2018).
- <sup>25</sup>P. A. Carpeggiani, G. Coccia, G. Fan, E. Kaksis, A. Pugžlys, A. Baltuška, R. Piccoli, Y. G. Jeong, A. Rovere, R. Morandotti, L. Razzari *et al.*, "Extreme Raman red shift: Ultrafast multimode nonlinear space-time dynamics, pulse compression, and broadly tunable frequency conversion," Optica 7, 1349–1354 (2020).
- <sup>26</sup>G. Fan, P. A. Carpeggiani, Z. Tao, G. Coccia, R. Safaei, E. Kaksis, A. Pugzlys, F. Légaré, B. E. Schmidt, and A. Baltuška, "70 mJ nonlinear compression and scaling route for an Yb amplifier using large-core hollow fibers," Opt. Lett. 46, 896–899 (2021).
- <sup>27</sup>R. Jung, J. Tümmler, and I. Will, "Regenerative thin-disk amplifier for 300 mJ pulse energy," Opt. Express 24, 883–887 (2016).
- <sup>28</sup> H. Fattahi, A. Alismail, H. Wang, J. Brons, O. Pronin, T. Buberl, L. Vámos, G. Arisholm, A. M. Azzeer, and F. Krausz, "High-power, 1-ps, all-Yb:YAG thin-disk regenerative amplifier," Opt. Lett. 41(6), 1126–1129 (2016).
- <sup>29</sup> M. Kaumanns, V. Pervak, D. Kormin, V. Leshchenko, A. Kessel, M. Ueffing, Y. Chen, and T. Nubbemeyer, "Multipass spectral broadening of 18 mJ pulses compressible from 13 ps to 41 fs," Opt. Lett. 43, 5877–5880 (2018).
- <sup>30</sup>Y. Wang, H. Chi, C. Baumgarten, K. Dehne, A. R. Meadows, A. Davenport, G. Murray, B. A. Reagan, C. S. Menoni, and J. J. Rocca, "1.1 J Yb:YAG picosecond laser at 1 kHz repetition rate," Opt. Lett. **45**, 6615–6618 (2020).
- $^{31}$ M. Kaumanns, D. Kormin, T. Nubbemeyer, V. Pervak, and S. Karsch, "Spectral broadening of 112 mJ, 1.3 ps pulses at 5 kHz in a  $LG_{10}$  multipass cell with compressibility to 37 fs," Opt. Lett. **46**, 929–932 (2021).
- <sup>32</sup> M. Dorner-Kirchner, V. Shumakova, G. Coccia, E. Kaksis, B. E. Schmidt, V. Pervak *et al.*, "HHG at the carbon K-edge directly driven by SRS red-shifted pulses from an ytterbium amplifier," ACS Photonics 10, 84–91 (2023).
- <sup>33</sup> A. M. Siddiqui, K. H. Hong, J. Moses, and F. X. Kärtner, "Bandwidth extension and conversion efficiency improvements beyond phase matching limitations using cavity-enhanced OPCPA," Opt. Express 29, 9907–9926 (2021).
- <sup>34</sup>M. Kretschmar, C. Brée, T. Nagy, A. Demircan, H. G. Kurz, U. Morgner, and M. Kovačev, "Direct observation of pulse dynamics and self-compression along a femtosecond filament," Opt. Express 22, 22905–22916 (2014).
- <sup>35</sup>V. Shumakova, P. Malevich, S. Ališauskas, A. Voronin, A. M. Zheltikov, D. Faccio, D. Kartashov, A. Baltuška, and A. Pugžlys, "Multi-millijoule few-cycle mid-infrared pulses through nonlinear self-compression in bulk," Nat. Commun. 7, 12877 (2016).
- <sup>36</sup>C.-H. Lu, W.-H. Wu, S.-H. Kuo, J.-Y. Guo, M.-C. Chen, S.-D. Yang, A. H. Kung, H. Kuo, J. Y. Guo, M. C. Chen, S. D. Yang, and A. H. Kung, "Greater than 50 times compression of 1030 nm Yb:KGW laser pulses to single-cycle duration," Opt. Express 27, 15638–15648 (2019).
- <sup>37</sup>M. Ueffing, S. Reiger, M. Kaumanns, V. Pervak, M. Trubetskov, T. Nubbemeyer, and F. Krausz, "Nonlinear pulse compression in a gas-filled multipass cell," Opt. Lett. 43, 2070–2073 (2018).
- <sup>38</sup>P. Balla, A. Bin Wahid, I. Sytcevich, C. Guo, A. L. Viotti, L. Silletti, A. Cartella, S. Alisauskas, H. Tavakol, U. Grosse-Wortmann, A. Schönberg *et al.*, "Postcompression of picosecond pulses into the few-cycle regime," Opt. Lett. **45**, 2572–2575 (2020).

- <sup>39</sup> P. Rußbüldt, J. Weitenberg, J. Schulte, R. Meyer, C. Meinhardt, H. D. Hoffmann, and R. Poprawe, "Scalable 30 fs laser source with 530 W average power," Opt. Lett. 44, 5222–5225 (2019).
- <sup>40</sup> A. L. Viotti, C. Li, G. Arisholm, L. Winkelmann, I. Hartl, C. M. Heyl, and M. Seidel, "Few-cycle pulse generation by double-stage hybrid multi-pass multi-plate nonlinear pulse compression," Opt. Lett. 48, 984–987 (2023).
- <sup>41</sup>G. Andriukaitis, T. Balčiūnas, S. Ališauskas, A. Pugžlys, A. Baltuška, T. Popmintchev, M. C. Chen, M. M. Murnane, and H. C. Kapteyn, "90 GW peak power few-cycle mid-infrared pulses from an optical parametric amplifier," Opt. Lett. 36, 2755–2757 (2011).
- <sup>42</sup> M. Nisoli, S. D. Silvestri, and O. Svelto, "Generation of high energy 10 fs pulses by a new pulse compression technique," Appl. Phys. Lett. 68, 2793–2795 (1996).
- <sup>43</sup>E. Conejero Jarque, J. San Roman, F. Silva, R. Romero, W. Holgado, M. A. Gonzalez-Galicia, B. Alonso, I. J. Sola, and H. Crespo, "Universal route to optimal few- to single-cycle pulse generation in hollow-core fiber compressors," Sci. Rep. 8, 2256 (2018).
- <sup>44</sup>G. Cerullo, M. Nisoli, S. Stagira, S. De Silvestri, G. Tempea, F. Krausz, and K. Ferencz, "Mirror-dispersion-controlled sub-10-fs optical parametric amplifier in the visible," Opt. Lett. **24**, 1529–1531 (1999).
- <sup>45</sup>M. Ouillé, A. Vernier, F. Böhle, M. Bocoum, A. Jullien, M. Lozano, J. P. Rousseau, Z. Cheng, D. Gustas, A. Blumenstein, P. Simon, S. Haessler, J. Faure, T. Nagy, and R. Lopez-Martens, "Relativistic-intensity near-single-cycle light waveforms at kHz repetition rate," Light: Sci. Appl. 9, 47 (2020).
- <sup>46</sup>F. Böhle, M. Kretschmar, A. Jullien, M. Kovacs, M. Miranda, R. Romero, H. Crespo, U. Morgner, P. Simon, R. Lopez-Martens, and T. Nagy, "Compression of CEP-stable multi-mJ laser pulses down to 4 fs in long hollow fibers," Laser Phys. Lett. 11, 095401 (2014).
- <sup>47</sup>S. Hädrich, M. Kienel, M. Müller, A. Klenke, J. Rothhardt, R. Klas, T. Gottschall, T. Eidam, A. Drozdy, P. Jójárt, and Z. Várallyay, "Energetic sub-2-cycle laser with 216 W average power," Opt. Lett. 41, 4332–4335 (2016).
- $^{\bf 48}$ B. E. Schmidt, P. Béjot, M. Giguère, A. D. Shiner, C. Trallero-Herrero, E. Bisson, J. Kasparian, J.-P. Wolf, D. M. Villeneuve, J.-C. Kieffer, P. B. Corkum, F. Légaré, P. B. Corkum, and F. Légaré, "Compression of 1.8  $\mu \rm m$  laser pulses to sub two optical cycles with bulk material," Appl. Phys. Lett. **96**, 121109 (2010).
- <sup>49</sup> R. Safaei, G. Fan, O. Kwon, K. Légaré, P. Lassonde, B. E. Schmidt, H. Ibrahim, and F. Légaré, "High-energy multidimensional solitary states in hollow-core fibres," Nat. Photonics 14, 733–739 (2020).
- M. Kumar, M. Arshadipirlar, R. Safaei, H. Ibrahim, and F. Légaré, "Generating ultrashort visible light pulses based on multidimensional solitary states in gas-filled hollow core fiber," APL Photonics 8, 056104 (2023).
  J. E. Beetar, M. Nrisimhamurty, T. C. Truong, G. C. Nagar, Y. Liu, J. Nesper,
- <sup>51</sup> J. E. Beetar, M. Nrisimhamurty, T. C. Truong, G. C. Nagar, Y. Liu, J. Nesper, O. Suarez, F. Rivas, Y. Wu, B. Shim, and M. Chini, "Multioctave supercontinuum generation and frequency conversion based on rotational nonlinearity," Sci. Adv. **6**, 5375 (2020).
- <sup>52</sup>G. Fan, R. Safaei, O. Kwon, V. Schuster, K. Légaré, P. Lassonde, A. Ehteshami, L. Arias, A. Laramée, J. Beaudoin-Bertrand, J. Limpert, Z. Tao, M. Spanner, B. E. Schmidt, H. Ibrahim, A. Baltuška, and F. Légaré, "High energy redshifted and enhanced spectral broadening by molecular alignment," Opt. Lett. 45, 3013–3016 (2020).
- <sup>53</sup>R. Safaei, O. Kwon, P. Lassonde, V. Cardin, E. Haddad, A. Leblanc, B. E. Schmidt, H. Ibrahim, and F. Légaré, "Low energy pulse compression in hollow core fibers using hydrofluorocarbon molecular gas," OSA Continuum 2, 1488–1495 (2019).
- <sup>54</sup>R. Safaei, "Towards the advanced high-energy multidimensional laser technology through harnessing the spatiotemporal nonlinear enhancement," Ph.D. Dissertation (Institut National de la Recherche Scientifique, Canada, 2020), pp. 58–59 Fig. 22.
- <sup>55</sup>J. K. Wahlstrand, Y. H. Cheng, and H. M. Milchberg, "Absolute measurement of the transient optical nonlinearity in N<sub>2</sub>, O<sub>2</sub>, N<sub>2</sub>O, and Ar," Phys. Rev. A **85**, 043820 (2012).
- <sup>56</sup>S. Zahedpour, J. K. Wahlstrand, and H. M. Milchberg, "Measurement of the nonlinear refractive index of air constituents at mid-infrared wavelengths," Opt. Lett. 40(24), 5794–5797 (2015).